Rock Mech Rock Eng
DOI 10.1007/s00603-011-0203-0

ORIGINAL PAPER

Prediction of the Bullet Effect for Rockfall Barriers: a Scaling Approach

M. Spadari · A. Giacomini · O. Buzzi · J. P. Hambleton

Received: 4 October 2011 / Accepted: 14 November 2011

Abstract The so-called "bullet effect" refers to the perforation of a rockfall protection mesh by impact of a small block, which has a kinetic energy lower than the design value, where the design value is determined through tests with relatively large blocks. Despite playing a key role in the overall performance of a flexible rockfall barrier, this phenomenon is still poorly understood at present. An innovative approach for quantitatively characterizing this effect based on dimensional analysis is proposed in this paper. The analysis rests on a hypothesis that the relevant variables in the impact problem can be combined into three strongly correlated dimensionless parameters. The relationship between these dimensionless parameters (i.e., the scaling relationship) is subsequently investigated and validated by means of data generated with a finite element model. The validation process shows that the dimensionless parameters are apt and that the proposed scaling relationship characterizes the bullet effect with a reasonable level of accuracy. An example from the literature involving numerical simulation of a full rock barrier is considered, and satisfactory agreement between the calculated performance of the barrier and that predicted by the established scaling relationship is observed.

Keywords Rockfall barrier · Kinetic energy · Bullet effect · Stress concentration · Dimensional analysis

M. Spadari · A. Giacomini · O. Buzzi (✉) · J. P. Hambleton
Centre for Geotechnical and Materials Modelling,
The University of Newcastle, Callaghan,
NSW 2308, Australia
e-mail: Olivier.Buzzi@newcastle.edu.au

1 Introduction

In many countries, rockfall represents a serious risk to people and infrastructures. Rockfall risks are mitigated either by stabilizing the rock mass or by installing protective systems such as engineered barriers, shelters, or earth dams. Among available protective systems, rockfall barriers, which typically consist of steel posts, cables, and a wire mesh, are attractive for the relative adaptivity of their design and the effective protection they provide over a broad range of impacting energy (Descoeudres et al. 1999). The impacting energy is usually determined as the sum of kinetic (translational) and rotational energy of the rock block at the instant just before it collides with the barrier. Both components of impacting energy are commonly obtained from numerical simulations of rockfall trajectories for the particular slope under consideration.

Protection barriers are usually tested to ascertain the threshold of impacting energy above which failure of the barrier will occur. This critical value of energy, or design value, is typically determined by means of experiments (Duffy and Smith 1990; Peila et al. 1998: Bertolo et al. 2009; Grassl et al. 2002; Hearn et al. 1995; Arndt et al. 2009), although numerical and analytical methods are increasingly being used to predict barrier performance (Anderheggen et al. 2002; Volkwein 2005; Cazzani et al. 2002; Cantarelli et al. 2008). Physical testing of barriers as they would be installed in the field is typically not a trivial exercise, and the free-fall test, a much simpler experiment, is often preferred to obtain an impact (Gerber 2001; EOTA 2008). In the free-fall test, where the rotational component of energy is negligible and total energy is solely kinetic, the impacting energy is determined simply by the block mass and drop height. In that case, a basic, unresolved question

Published online: 29 November 2011

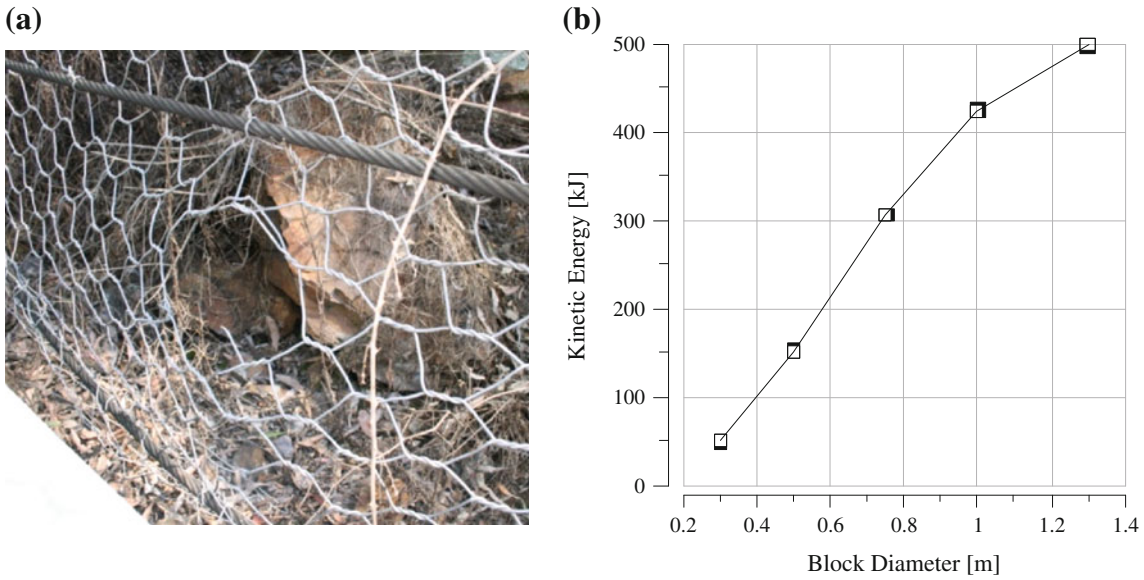

Fig. 1 Examples of the bullet effect: **a** perforated rockfall mesh, **b** kinetic energy at failure of a rockfall barrier for different block sizes (adapted from Cazzani et al. (2002))

arises as to which combination of block mass and velocity should be used to achieve the desired impacting energy for the test. The Swiss design guidelines (Gerber 2001), for example, require using not one but multiple block dimensions, including small sizes, for the approval of a rockfall protection kit. This is motivated by the fact that a small block impacting at high speed may perforate a barrier despite having a kinetic energy lower than the critical value determined from tests involving a large block. More generally, there is a size effect when dealing with impact of blocks on a barrier. This effect is usually referred to as the "bullet effect" in the literature and it has been mentioned by a number of researchers (Cazzani et al. 2002; Cantarelli et al. 2008; Giani 1992; de Col and Cocco 1996; Volkwein et al. 2005; Buzzi et al. 2011).

Figure 1 shows two manifestations of the bullet effect. A typical failure in a steel wire mesh due to impact of a small block can be seen in Fig. 1a, where a block with a diameter of roughly 30 cm has impacted a rockfall barrier between two horizontal cables and has perforated the mesh. As discussed by De Col and Cocco (1996), failures of this kind are usually localized in small areas of the mesh and do not involve structural elements such as posts and cables. Figure 1b shows the results obtained from a numerical model developed by Cazzani et al. (2002). The dependence of the mesh performance on the block size clearly appears: the smaller the block, the smaller is the impacting energy at failure. This raises the issue of the relevance of kinetic energy as a design criterion, since it is evident that there is no single value of kinetic energy (i.e., a design value) that effectively defines a barrier's ability to withstand impacts over a range of block sizes.

Interestingly, numerical models can reproduce the loss of performance associated with the bullet effect (Cazzani et al. 2002; Buzzi et al. 2011), but the origin of the phenomenon is seldom analyzed. It is generally conjectured that this phenomenon is the result of stress concentration. Quite recently, Buzzi et al. (2011) developed a numerical model of block impact on a wire mesh and conducted some analysis to investigate the idea of stress concentration. The authors came to the conclusion that the progressive loss of performance of a mesh can be related to a lower number of wires entering into plasticity as the block size decreases. Consequently, the wires elongate more to absorb the energy and reach failure quicker. However, this failure mechanism is partly a consequence of the modeling assumptions (e.g., material behavior and mesh connections), and it is unsure if such a mechanism would prevail in practice.

Despite the relevance of the bullet effect for the design and performance of rockfall protective systems, there is a clear lack of data in literature on this topic. More critically, there is currently no efficient predictive method that could be used to estimate the performance of a barrier for different sizes of impacting blocks. Extensive physical testing or numerical modeling can potentially be employed to check the barrier performance; however, such a process is very time-consuming on account of not only the repetitions required at various block sizes, but also the iterations necessary to determine the block speed inducing failure at a particular block size. A more efficient approach requiring a fewer tests or lower computational cost is clearly needed.

It is herein proposed to use dimensional analysis to characterize the performance of a barrier in terms of the

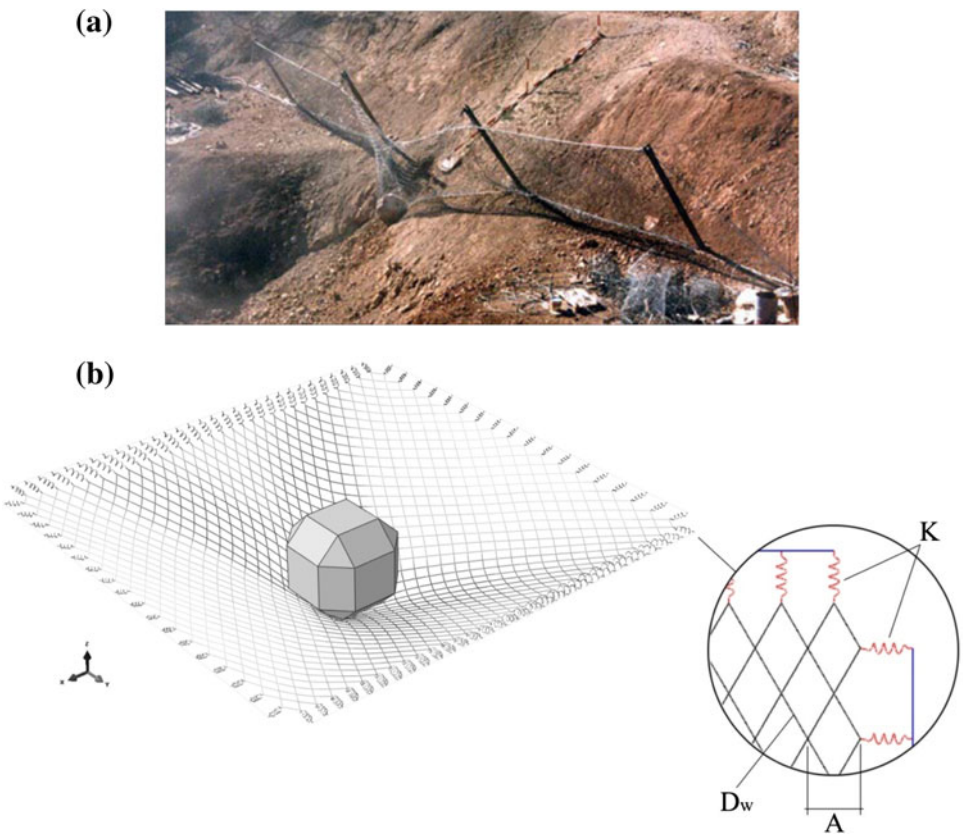

Fig. 2 **a** Photograph of a rockfall barrier after Peila and Oggeri (2005). **b** Idealized rockfall impact problem used for the numerical model showing aperture A, spring stiffness K, and wire diameter D_w

bullet effect. In the first part of the paper, dimensionless parameters pertaining to a rock block impacting the wire mesh within a rockfall barrier are derived after due identification of the relevant physical variables. The second part of the paper presents the results of a numerical model that has been developed using Abaqus 6.10 to create a database of the responses of different meshes to the impact of blocks of various sizes. Finally, the scaling relationships determined through dimensional analysis and the numerical results are validated by comparison with results obtained in a previous study for a full barrier. The results suggest that the bullet effect can be satisfactorily characterized by three essential dimensionless parameters containing the relevant variables of the problem. For the first time, a network of performance curves, referred to as the "Rockfall Barrier Performance Model", or RoBaP Model, is produced and used to capture the dependence of the barrier performance on the block size.

2 Definition of the Physical Problem

Before conducting the dimensional analysis, an idealization of the rockfall impact problem is first described in relation to real rockfall protection systems, and the relevant physical variables to be included in the analysis are identified.

Figure 2a shows a rockfall barrier and how it can deform upon impact. The design of a barrier is not unique, though it invariably revolves around several critical elements: foundations, posts, an intercepting structure (steel mesh), and cables. Usually, the part of mesh located between two successive posts is referred to as a "module". It can be seen in Fig. 2a that the mesh is not necessarily attached to all posts, which are mainly used to support the cables.

The performance of a barrier upon impact is affected by many variables. Some play a major role, while others have a minor effect. For example, the coefficient of friction between the mesh and the block, the Poisson's ratio of the steel mesh, and the mechanical properties of the block (which typically does not fail upon impact) are here considered to have negligible effect. On the contrary, dimensions of the block, strength of the steel mesh, mesh geometry and, last but not least, the stiffness of the system all play a major role in the response of a rockfall barrier. As a concept, "stiffness" refers to the extent to which the barrier deforms upon impact. Interestingly, despite being a crucial property of a rockfall barrier, stiffness is seldom quantified on account of the many underlying factors that influence this property. Among other factors, the overall stiffness comes from the type of mesh (chain link or double twist), deformability and ductility of steel, distance

between posts, length and height of the mesh, the effect of energy dissipators (if present), the means by which the posts and cables are supported, and the number of cables.

For the present study, concerning perforation of only a small portion of the mesh in a rockfall barrier, the independent factors that lead to the overall stiffness of the barrier are irrelevant. That is, the full rockfall barrier need not be considered in the analysis, and the free-fall impact problem can be regarded as a block impacting a segment of mesh that is somehow supported at the periphery by springs of effective (nonlinear) stiffness, which in general may vary specially over the region of support. By viewing the problem in this way, no approximation has yet been made, although it is clear that the degree to which the idealized problem represents a real rockfall barrier depends on the assumed position and stiffness of the springs. In this paper, we assume for simplicity that the springs possess constant linear stiffness, denoted by K, and they support a rectangular region of mesh at regular intervals, as shown in Fig. 2b. The merit of assuming constant linear stiffness is in the resulting simplification of the analysis, although some comments as to the determination of K for real systems is presented in the prediction exercise at the end of the paper (Sect. 7). The rectangular region of mesh has height H and length $L > H$. It will be shown in Sect. 4 that H is the key dimension in the impact problem, and H alone is therefore included as a relevant variable in further analysis.

The configuration for the wire mesh is also shown in Fig. 2b. The mesh is chain link (elementary cell of diamond shape) as opposed to a double twist (elementary cell of hexagonal shape), and each cell in the mesh is a diamond (rhombus) whose shorter diagonal has length denoted by A, where A is referred to as "aperture". The shape of the diamond corresponds to an existing rockfall mesh. The wire itself has a diameter D_w, and it is assumed as in the work of Cazzani et al. (2002) that the material is elastic-perfectly plastic with yield strength σ_y and a specified failure strain. As discussed in Sect. 4, elastic properties of the wire and the failure strain are held constant in the analysis. Furthermore, the elastic properties of the wire are seen as having secondary importance in the block impact problem, and the failure strain is already a dimensionless parameter. These quantities, as well as the density of the wire, are therefore excluded here as explicit variables.

The shape of the impacting block, which is in accordance with testing recommendations from ETAG 027 (EOTA 2008), is shown in Fig. 2b. The nominal length of the block's edges is denoted by D_b. With the dimension defined in this way, the block density suffices to fully characterize the rigid block. The block density is denoted by ρ, and throughout the paper a constant value of $\rho = 2{,}400$ kg/m^3 is assumed since the variability of density of natural dense rocks is fairly low (Cazzani et al. 2002).

The performance of the idealized system is expressed in terms of critical speed v, which is the minimum speed required for a given block to perforate the mesh. On the basis of the considerations above, it is implicitly assumed that there exists some function f that relates v to the remaining primary variables:

$$v = f\left(\rho, K, \sigma_y, H, A, D_b, D_w\right) \tag{1}$$

where ρ is the block density, D_b its characteristic length, H the mesh height, A its aperture, D_w the wire diameter, σ_y the material strength, and K the stiffness of the system.

3 Dimensional Analysis of Block Impact on a Barrier

Dimensional analysis rests on the Buckingham Pi Theorem (Buckingham 1914), which states that a physical problem involving N independent variables and P dimensions can be reformulated using N–P dimensionless parameters. The main motivation of performing dimensional analysis is to reduce of the number of parameters required to describe a problem (Langhaar 1951). As a convention, physical (dimensional) quantities as defined in Sect. 2 are referred to as "variables" throughout the paper, whereas the dimensionless groups of variables are referred to as "dimensionless parameters".

Equation 1, which describes the physical problem of interest, involves eight variables and three dimensions (time, length, and mass). According to the Buckingham Pi theorem, Eq. 1 can be re-written using only five dimensionless parameters. These five dimensionless parameters are not, however, uniquely determined by the dimensions of the eight original variables alone. In this paper, the analysis proceeds by first postulating the key dimensionless parameters and then using the numerical model to assess their validity.

By analogy to other impact problems in solid mechanics (Li and Jones 2000; Johnson 1972), it is proposed to group the critical speed, the stiffness of the system and the height of the mesh in the first dimensionless parameter, E^*, as follows:

$$E^* = \frac{\rho v^2 H}{K} \tag{2}$$

The parameter E^* bears similarity to the "damage number" used by Johnson (1972), with the main differences being that ρ is the density of the impacting block (as opposed to the material with which it collides), and the stiffness of the barrier, rather than the yield strength, appears in the denominator. Parameter E^* is the descriptor of barrier performance in terms of critical speed, and it is hence referred to as the "performance parameter". It should be noted that E^* does not directly relate to kinetic

energy (i.e., 0.5 mv^2, where m is block mass), but rather to the square of critical speed.

It is assumed that the second fundamental dimensionless parameter should quantify the stiffness of the barrier in relation to the yield strength of the wire. This parameter, denoted by S^* and referred to as the "strength-stiffness parameter", is therefore chosen as

$$S^* = \frac{K}{H\sigma_y} \tag{3}$$

Large values of S^* imply that the barrier is relatively stiff, and deformation of the barrier prior to the onset of yielding is small. Conversely, small values of S^* imply that large deformation will occur prior to failure.

Parameters E^* and S^* are independent of the characteristic length of the block, D_b, as well as the two parameters pertaining to the geometry of the mesh, D_w and A. Rather than defining three independent dimensionless parameters to account for the influence of these parameters (e.g., D_b/H, D_w/H, and A/H), it is hypothesized that D_b, D_w, and A can be combined in a single dimensionless parameter, called the "geometrical parameter" and defined as

$$G^* = A^a D_b^b D_w^c \tag{4}$$

where the exponents a, b, and c are as yet unknown but satisfy the following condition, as required for dimensional homogeneity:

$$a + b + c = 0 \tag{5}$$

The strong assumption that D_b, D_w, and A can be lumped together in a single dimensionless parameters is made with the expectation that stress concentrations are determined by the local geometry of the mesh in relation to the block size. This hypothesis is tested in due course in the paper.

The dimensionless parameters proposed in this section potentially form the basis for the following simple alternative to Eq. 1:

$$E^* = F(S^*, G^*) \tag{6}$$

In accordance with the literature on dimensional analysis and similitude, Eq. 6 is here referred to as the "scaling relationship" for a block impacting a barrier. Rather than identifying f, a function of seven variables in Eq. 1, the task is now to identify F in Eq. 6, a function of only two parameters. It remains to be shown, however, that Eq. 6 provides a reasonable approximation to the data available for block impact on a barrier. Toward this purpose, the remainder of the paper is dedicated to validation of Eq. 6 and the dimensionless parameters involved. In the present study, the data used to validate Eq. 6 is generated using an upgraded version of the numerical model developed by Buzzi et al. (2011). An outline of this model is presented in the next section.

4 Numerical Model

With a view toward investigating the soundness of Eq. 6 and the dimensionless parameters E^*, S^*, and G^*, numerical simulations of free-fall tests were performed using the dynamic finite element code Abaqus/Explicit 6.10. This section presents a broad overview of the numerical procedure and underlying assumptions.

4.1 Geometry

As discussed in Sect. 2, the numerical model is an idealization of a free-fall test on a full rockfall protection barrier. It consists of a concrete block impacting vertically and centrally on a steel mesh (Fig. 3). The mesh was connected to rigid supports by means of springs of stiffness K, which were added to the initial model developed by Buzzi et al. (2011) to artificially vary the stiffness of the idealized system. Rather than simulating the initial gravitationally induced free fall, the block was placed in contact with the mesh in the simulations and given a prescribed initial velocity combined with gravitational loading to reproduce the whole impact.

4.2 Mesh and Elements

The impacting block was made of four-node tetrahedral elements (C3D4), and the steel wires were discretized using two-node linear 3-D beam elements (B31). The beam elements had a circular section of diameter D_w and were rigidly connected at the nodes. Only one element was used per diamond side. This choice might affect the results in terms of matching experimentally observed mesh behavior, but such a potential error is immaterial for the comparative study of performance conducted in this paper. The springs were inserted as connector elements between the outer nodes and a support beam, which was constrained in displacement and rotation.

4.3 Material and Contact Properties

In the present study, it is assumed that the impacting block does not fail. Consequently, the block in the numerical simulations was composed of elastic material with parameters representative of concrete or rock ($E = 30$ GPa, $v = 0.3$ and $\rho = 2{,}400$ kg/m^3). As discussed in Sect. 2, elastic-perfectly plastic behavior ($E = 210$ GPa, $v = 0.3$ and variable yield strength σ_y) was assumed for the steel of the mesh, which had a density of 7,800 kg/m^3. In the

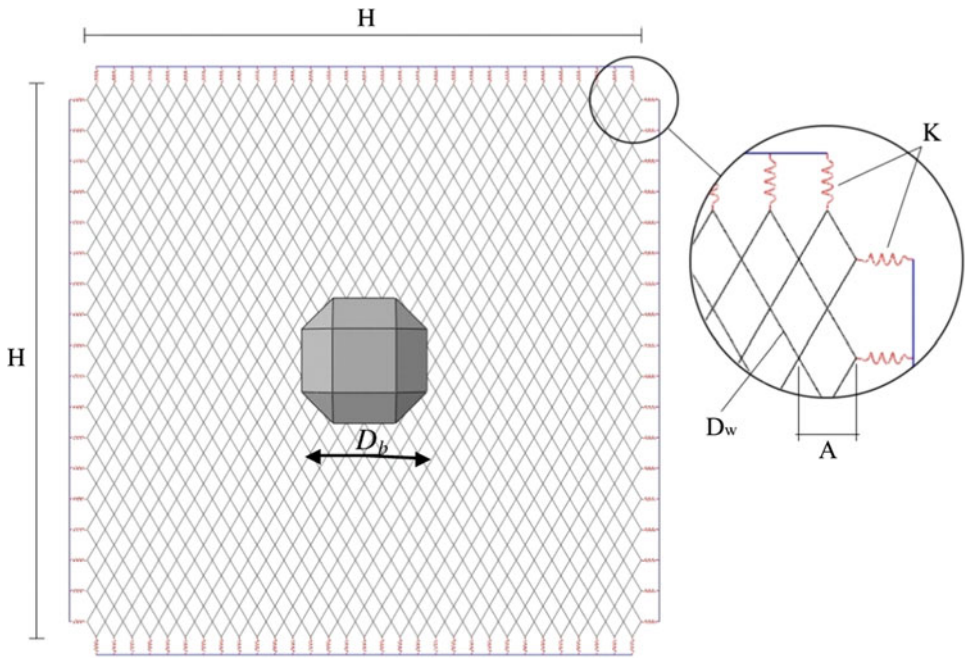

Fig. 3 Plan view of the numerical model developed in Abaqus showing height of the mesh H, stiffness of a single spring K, aperture of the mesh A, and diameter of the wire D_w. The block impacts the mesh in its center and has an initial velocity orthogonal to the page

simulation, element failure happens instantaneously when the plastic strain at failure ε_p^f is reached. Throughout the simulations, $\varepsilon_p^f$was set at 10%, which is large for steel. The assumed value comes from the calibration against experimental results of free-fall tests (Buzzi et al. 2011), where it was found that a large value of ε_p^f could compensate for errors introduced when simplifying the true boundary conditions by springs of constant stiffness. A more realistic (lower) value would certainly change, but not compromise, the results. Finally, dry friction with coefficient of friction 0.3 was specified as the contact interaction between the mesh and the block.

4.4 Typical Results

Critical velocity v was evaluated for roughly 80 different combinations of the variables appearing in Eq. 1. For each particular choice of variables, the critical velocity was iteratively determined by running three to four simulations with varying initial velocity. Hence, around 300 simulations were conducted. Figure 4 shows the deformed mesh (in perspective and side view) before and after failure from a simulation where velocity was set to the critical value v. The deformation and failure pattern are in good agreement with experimental tests (Buzzi et al. 2011). Figure 4a also shows the stress pattern within the mesh, where the darker shades of gray indicate higher axial stress. It can be seen that the impact generates a cross-shaped distribution of axial stress in which the cross aligns with the strands of the mesh. Such a stress distribution was already observed by Anderheggen et al. (2002).

Figure 4 pertains to a mesh with $H = L = 2.5$ m. Plotting the tensile stress distribution on a larger mesh, such as the mesh shown in Fig. 5 where $H = 2.5$ m and $L = 5$ m, highlights that the height of the mesh is critical in terms of stress distribution. It can be seen that the extra length of mesh when extended from 2.5 to 5 m does not carry much of the tensile stress generated by the impact.

5 Overview of the Validation Steps for the Scaling Relationship

The validation of the three dimensionless parameters and the evaluation of the function F in Eq. 6 were achieved in successive steps. These steps are described in the following and summarized in Table 1, which indicates quantities that were varied (V), maintained constant (C) or determined as the result of the simulation (R). As shown in the table, different groups of influencing variables were varied one at a time to conduct a rigorous and thorough validation. This was done for both the largest and the smallest block considered in the analysis ($D_b = 0.65$ m and $D_b = 0.25$ m, respectively).

In the first phase of the validation (discussed in Sect. 6.1), the geometric parameters appearing in G^* were viewed as fixed, and the relationship between E^* and S^* was assessed. This was conducted in three steps (steps 1–3 in Table 1). In step 1, three values of stiffness were combined with three values of strength for each of the two blocks. This led to nine data points used to determine if a correlation could be established between E^* and S^*. The robustness of the correlation was then tested either by

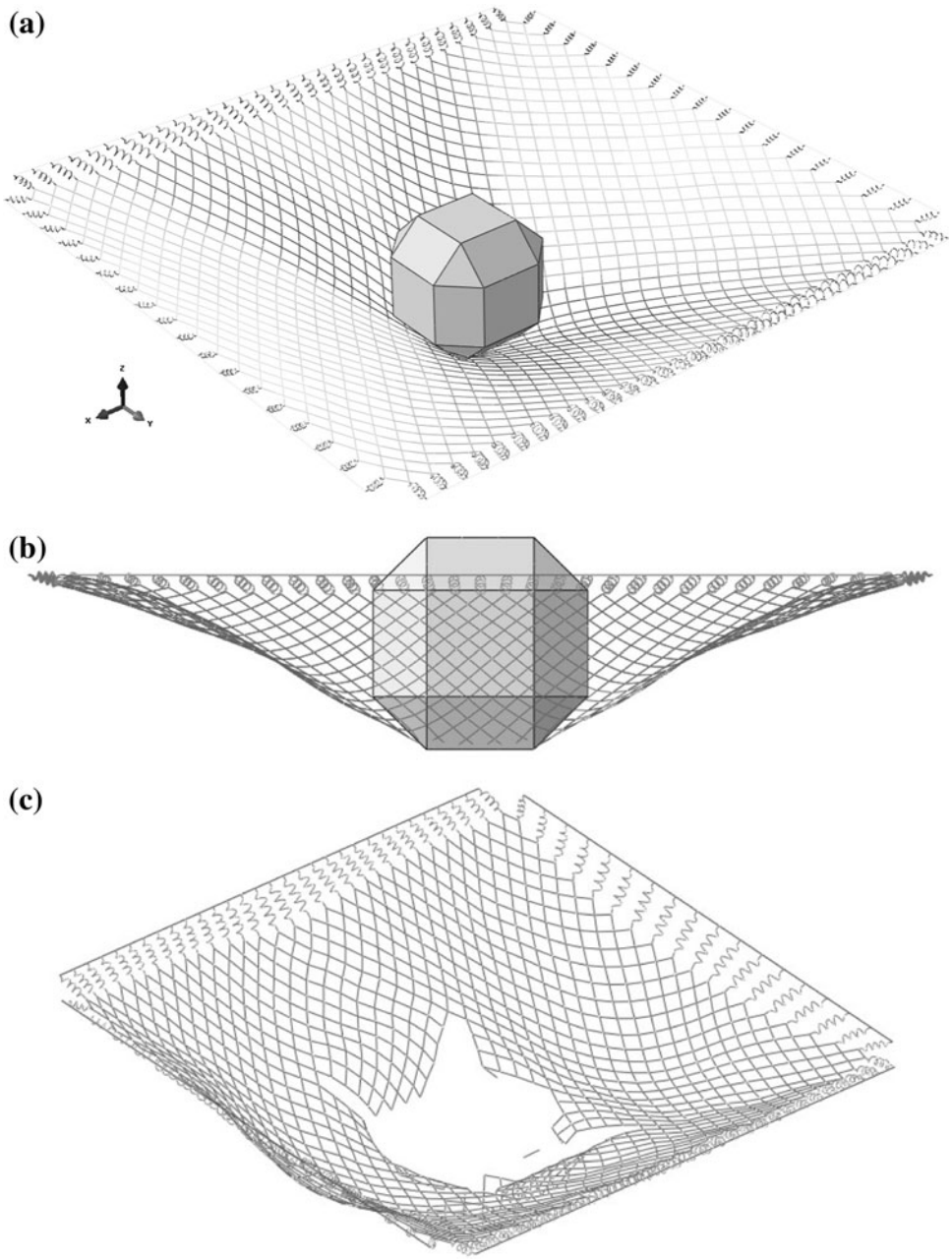

Fig. 4 **a** View of the deformed mesh just before failure. The shade of *gray* indicates the level of axial stress in the wires (*light gray* stress lower than 500 MPa; *dark gray* stress from 500 to 1,500 MPa). **b** Side view of deformed mesh just before failure. **c** View of the failure pattern (level of stress not indicated on this subfigure). Mesh of 2.5 per 2.5 m

investigating multiple combinations of stiffness and strength yielding the same value of S^* (step 2) or by introducing different mesh dimensions (step 3).

In the second phase (discussed in Sect. 6.2), the exponents appearing in G^* (Eq. 4) were evaluated, and the function F was partly defined. The validation of G^* involves, first and foremost, identification of the unknown exponents a, b and c in Eq. 4. Instead of guessing the possible combinations satisfying dimensional homogeneity (Eq. 5), back analysis was performed to identify the exponents in a more rigorous and systematic manner. To accomplish this, different combinations of block size and wire diameter yielding the same mesh performance were determined (step 4 in Table 1). This provided information about exponents b and c. Lastly, the value of a was deduced from the condition of dimensional homogeneity, and the overall validity of values determined for exponents a, b, and c was checked in step 5.

6 Validation of the Proposed Scaling Relationship

6.1 Validation of E^* and S^*

The first step of the validation of the proposed scaling relationship (Eq. 6) was to determine whether a

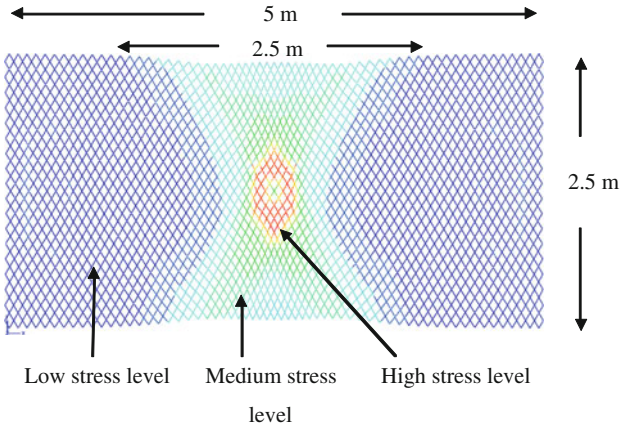

Fig. 5 Distribution of axial stresses within wires for mesh with $H = 2.5$ m and $L = 5$ m upon impact ($D_b = 0.65$ m, $K = 50$ kN/m, $\sigma_y = 1{,}600$ MPa)

Table 1 Variations of the parameters and corresponding figures for the different steps of validation (V varied, C constant, and R result)

Validation of	Step	Figure	K	σ_y	H	A	D_w	D_b	v
E^*–S^*	1	6, 7	V	V	C	C	C	C	R
E^*–S^*	2	8	V	V	C	C	C	C	R
E^*–S^*	3	9	C	C	V	C	C	C	R
G^*	4	10	C	C	C	C	R	V	C
G^*	5	11	C	C	C	V	V	C	R

satisfactory correlation could be obtained between E^* and S^* for fixed values of the variables appearing in G^* (Eq. 4). In addition to the critical velocity v, four parameters appear in E^* and S^*: density of the block ρ, stiffness K, yield strength σ_y, and the mesh height H. As discussed in Sect. 2, ρ does not vary substantially between various types of rock and concrete, and it was therefore considered fixed ($\rho = 2{,}400$ kg/m^3). On the other hand, K and σ_y are highly variable, and to investigate the validity of Eq. 6, these parameters were varied independently. The effect of varying H is considered later in this section.

Figure 6 shows the result of the simulations for the largest and smallest blocks considered in the analysis ($D_b = 0.65$ and 0.25 m, respectively), where simulations were run at constant aperture ($A = 70$ mm), constant wire diameter ($D_w = 3$ mm), constant mesh height ($H = L = 2.5$ m), and the nine combinations of K and σ_y from Table 2. Figure 6 displays a clear linear correlation (on a log–log scale) between E^* and S^* for the two different block sizes, with relatively small scatter about the corresponding trend lines. This suggests that E^* and S^* are appropriate dimensionless parameters for characterizing the critical block velocity with fixed geometric parameters for the mesh (i.e., fixed G^*). Figure 7 shows similar trend lines evaluated for each of the block sizes considered

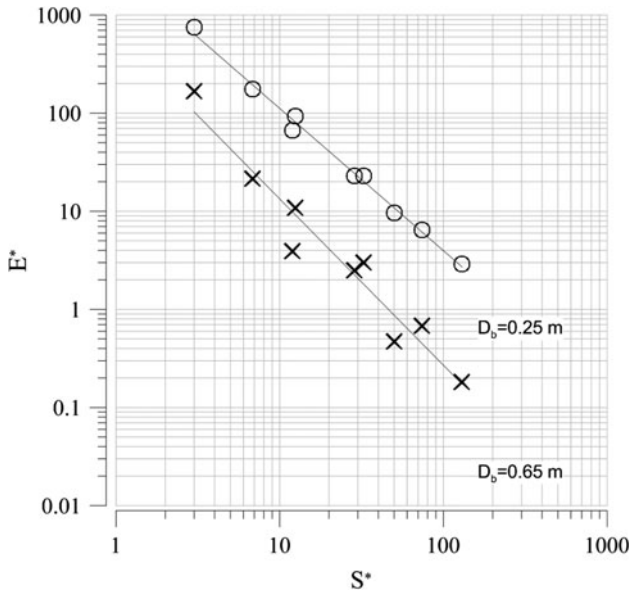

Fig. 6 E^* versus S^* for two blocks ($D_b = 0.25$ and 0.65 m) and for nine different combinations of K and σ_y. *Power trend lines* are also shown, where correlation coefficients are $R^2 = 0.94$ and 0.99 for $D_b = 0.65$ and 0.25 m, respectively

($D_b = 0.25$, 0.35, 0.4, 0.55 and 0.65 m). For clarity, the data points are omitted in the figure.

Each trend in Fig. 7 corresponds to a given block size, and it should be recalled that the simulations were run at constant aperture ($A = 70$ mm) and wire diameter ($D_w = 3$ mm). Consequently, as per Eq. 4, the trends presented in Figs. 6 and 7 are evolutions at constant G^*.

For each trend in Fig. 7, low values of S^* correspond to high strength and/or compliant systems. Consequently, the critical speed required for a block to perforate the mesh is high. On the other hand, when reducing the mesh strength and/or stiffening the system (high values of S^*), the critical speed decreases. This behavior is consistent with experimental observations. Also, the relative position of the trends is consistent with findings from experiments: for a given system (i.e., for a given S^*), the smaller the block, the higher the critical speed required (i.e., E^*). Note that the existence of the bullet effect cannot be evidenced from these trends alone, since higher speed is always required to perforate a mesh as the blocks get smaller, even without bullet effect. The manifestation of the bullet effect in the proposed scaling relationship is discussed in the last section of the paper. The network of curves as shown in Fig. 7 is here referred to as the "Rockfall Barrier Performance Model" or, more simply, the RoBaP Model.

For E^* and S^* to be appropriate dimensionless parameters, E^* should remain constant as K and σ_y are varied in proportion to one another (i.e., constant S^*). To verify this, additional simulations in which the same factor α was

Table 2 Values of stiffness K and steel strength σ_y, used for the first step of validation

K (kN/m)	σ_y (MPa)
12, 50 and 130	400, 700 and 1,600

Nine combinations of K and σ_y were created from these values, leading to nine values of S^*. Other parameters were kept constant: $H = L = 2.5$ m, $D_w = 3.0$ mm, and $A = 70$ mm

Table 3 Reference values of stiffness and yield strength, as well as corresponding values of S^*, used for validation of E^* and S^*

K_0 (kN/m)	σ_{y0} (MPa)	S^*
12	1,600	3
50	1,600	12.5
130	700	74.3
130	400	130

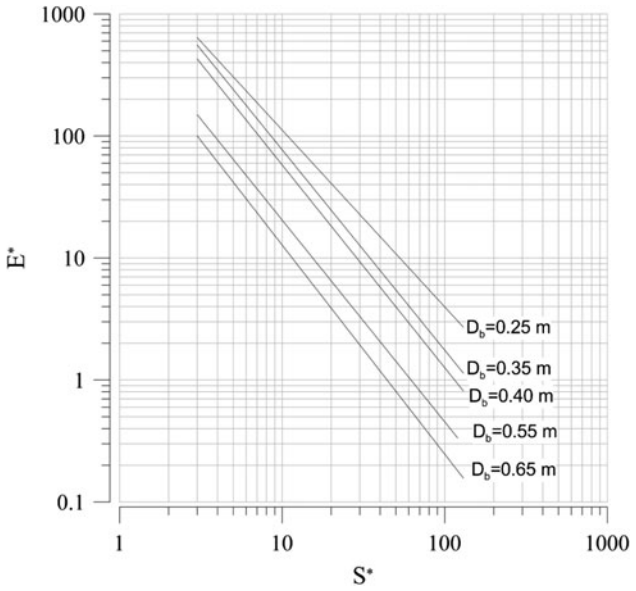

Fig. 7 *Trend lines* showing E^* versus S^* for all different values of D_b

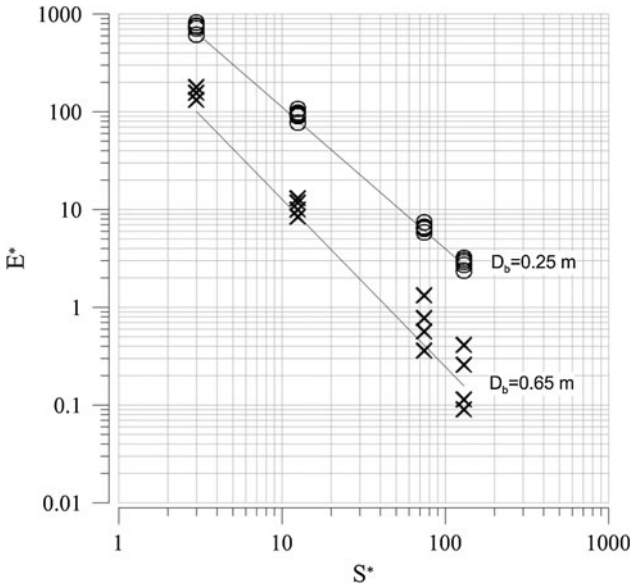

Fig. 8 Verification of the correlation between E^* and S^* with multiple combinations of K_0/σ_{y0} and α ($H = 2.5$ m, $D_w = 3.0$ mm, and $A = 70$ mm)

applied to both stiffness and yield strength were performed, where the factors α were selected so that

$$S^* = \frac{K}{L\sigma_y} = \frac{(\alpha K_0)}{L(\alpha\sigma_{y0})}, \quad \alpha \in \{0.5,\ 0.8,\ 1.4,\ 2.2\} \tag{7}$$

In Eq. 7, K_0 and σ_{y0} are reference values of stiffness and yield strength that determine the value of S^*. Four different values of S^* (i.e., four pairs of K_0 and σ_{y0}) were considered, as shown in Table 3. By focusing only on the smallest and largest blocks, a total of 32 data points were generated in this way to validate the correlations between E^* and S^* observed in Fig. 7.

Figure 8 shows E^* determined from simulation at each of the value of S^* and α considered. In most cases, similar values of E^* were obtained at each different value of α. Some scatter is evident, however, for the largest block ($D_b = 0.65$ m) with $S^* = 74.3$ and 130. The reason behind these deviations is unknown at present, but it is speculated that edge effects (boundary conditions) play a role at these points on account of the large size of the block combined with high stiffness. Nevertheless, the results shown in Fig. 8 basically confirm the existence of a relationship between E^* and S^* and the possibility of quantifying the bullet effect in terms of dimensionless parameters instead of physical variables. It should be emphasized that the trend lines shown in Fig. 8 are the same as those from Fig. 6, implying that the previously established correlations between E^* and S^* are quantitatively correct.

Up to this point, the mesh height H had been constant in the analysis. This parameter appears in both E^* and S^*, and it is therefore of interest to determine whether varying H independently affects (i.e., maintains or destroys) the correlation between these two dimensionless parameters. In addition to the initial mesh configuration (2.5 × 2.5 m), three other configurations were considered: 1 × 1 m, 2.5 × 5 m and 5 × 5 m. Parameters K and σ_y were kept constant, with $K = 50$ kN/m and $\sigma_y = 1{,}600$ MPa, and block sizes were again $D_b = 0.65$ and 0.25 m. The smallest mesh was not tested with the largest block, as significant edge effects were expected.

Figure 9 shows the performance of the three mesh configurations, where it can be seen that the results fall on, or very close to, the trend lines obtained with the initial mesh. This confirms that E^* and S^* are suitable dimensionless parameters exhibiting a strong correlation. Indeed, all physical parameters in E^* and S^*, apart from the

material density, have now been varied independently in the analysis, and each time the same relationship between E^* and S^* was obtained with reasonable accuracy.

6.2 Validation of G^*

For G^* and the proposed scaling relationship to be valid, the relationship between E^* and S^* should remain unchanged when the parameters appearing in the definition of G^* (aperture A, wire diameter D_w, and block diameter D_b) are varied independently, but G^* itself remains constant. As a first step toward identifying the exponents in the definition of G^*, we first consider the combinations of D_w and D_b that lead to constant values of E^* and S^* when A is constant.

Using the results of the simulation with $A = 70$ mm, $D_w = 3$ mm, $H = 2.5$ m, $K = 50$ kN/m, $\sigma_y = 1{,}600$ MPa, and $D_b = 0.65$ m as a basis, a number of simulations were performed to ascertain the manner in which block size and wire diameter should be simultaneously reduced or increased to maintain the mesh performance ($E^* = 10$). Three block size sizes ($D_b = 0.25$, 0.35 and 0.55 m) were considered in addition to the initial diameter of $D_b = 0.65$ m, and the three corresponding wire diameters required to give $E^* = 10$ were iteratively evaluated. This process, which pertained to $S^* = 12.5$, was then repeated with $S^* = 74.3$ ($H = 2.5$ m, $K = 50$ kN/m, $\sigma_y = 1{,}600$ MPa), and this yielded another three wire diameters that were found to be approximately equal to those calculated previously (Fig. 10a). Finally, the whole analysis was repeated starting from a small block ($D_b = 0.25$ m) and progressively increasing the block size (Fig. 10b). Again, the wire diameter D_w required to maintain constant E^* was found to be relatively insensitive to S^*, which is consistent with the proposed scaling relationship of Eq. 6.

It can be seen in Fig. 10 that there is a strong correlation between the block size D_b and the wire diameter D_w required to furnish constant E^* at specified S^*. Furthermore, the points in Fig. 10 can be satisfactorily fitted with a

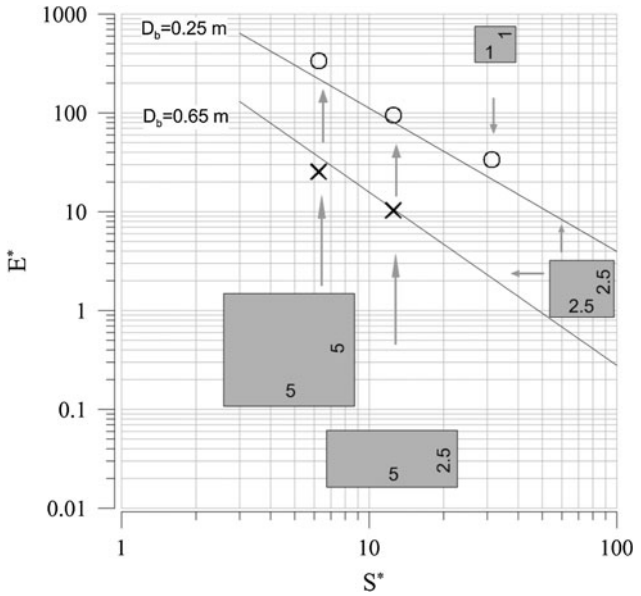

Fig. 9 Influence of mesh height H on the correlation between E^* and S^*. The *gray shapes* indicate the mesh shape and dimensions. H is defined as the shortest dimension

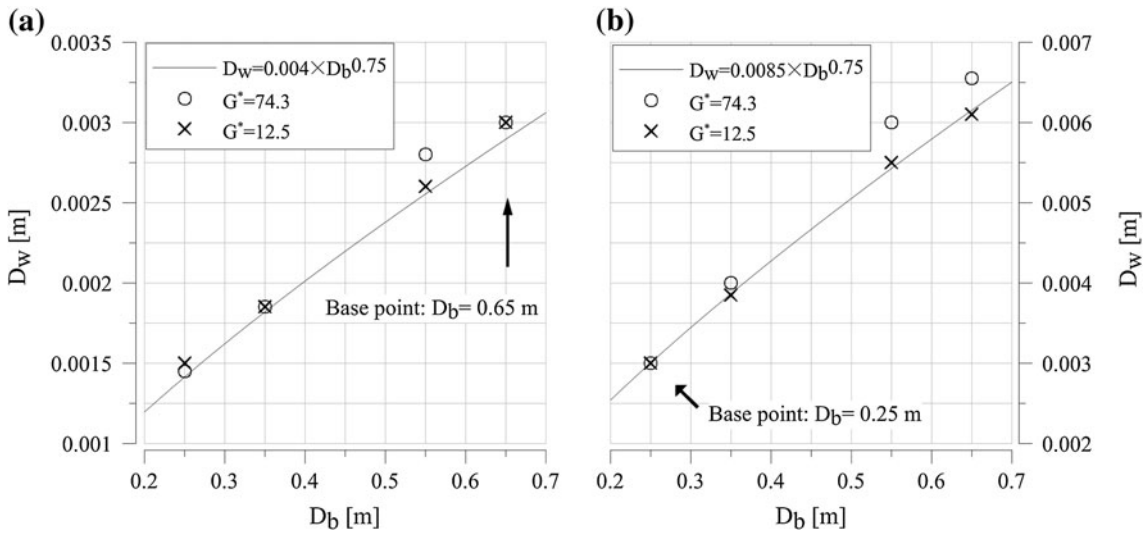

Fig. 10 Values of wire diameter D_w required for each block size D_b so that E^* is maintained constant. The analysis was performed starting from $D_b = 0.65$ m with a progressive reduction of the block size (**a**), and from $D_b = 0.25$ m with a progressive increase of the block size (**b**). For each initial block size, two mesh configurations were considered ($S^* = 12.5$ and 74.3). Aperture of the mesh is constant ($A = 70$ mm)

Table 4 Values of aperture A and wire diameter D_w used for the final step of validation of G^*

D_b (m)	D_w (mm)	A (mm)	G^*
0.65	3	70	0.008
0.65	2.64	50	0.008
0.65	2.32	30	0.008
0.25	3	70	0.0164
0.25	2.64	50	0.0164
0.25	2.32	30	0.0164

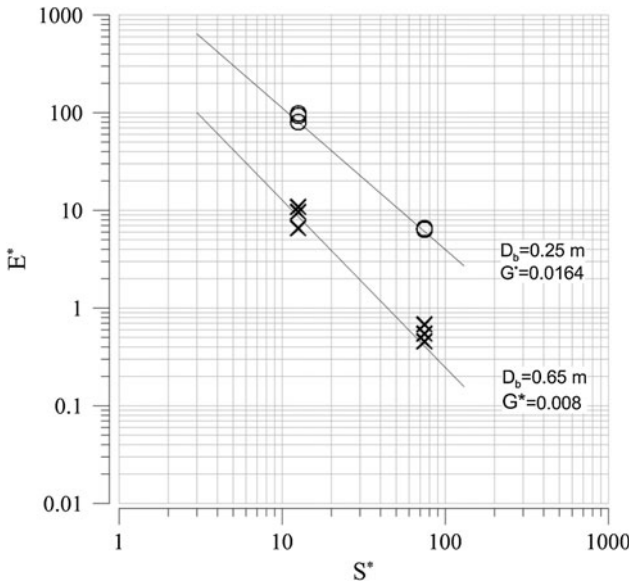

Fig. 11 Correlation between E^* and S^* for various combinations of mesh aperture A, wire diameter D_w, and block size D_b leading to $G^* = 0.008$ and 0.0164

power-type curve, which can be written, for both values of S^*, as

$$D_w D_b^{-3/4} = \eta \tag{8}$$

where η is a constant. Since the aperture A is considered constant in the back analysis, it does not explicitly appear in Eq. 8; however, its effect can be accounted for in the constant η. Namely, Eqs. 5 and 8 can be combined to find $\eta = G^* A^{1/4}$ and

$$G^* = \frac{D_w}{D_b^{3/4} A^{1/4}} \tag{9}$$

To fully assess the validity of G^* as defined in Eq. 9, three different mesh apertures A were considered, and the wire diameter was adjusted to keep G^* constant (Table 4). Simulations were performed with $S^* = 12.5$ and 74.3, as previously considered, and corresponding values of E^* were computed. The results are shown in Fig. 11, which also plots the trends determined in Sect. 6.1. The computed values of E^* fall close to the previously established trend lines, where unique values of G^* can now be assigned to each line. Figure 11 confirms that G^*, as defined in Eq. 9, is an appropriate dimensionless parameter. Namely, parameters A, D_w, and D_b can vary independently, but only their combination as it appears in G^* affects the relationship between E^* and S^*.

By qualitative comparison with experiments, the physical meaning behind G^* is also sound. For a given S^* (given strength and stiffness), a higher G^* results in higher E^* (higher critical speed). An increase of G^* can result not only from a decrease in block size, which is the origin of the bullet effect, but also from a decrease of mesh aperture or an increase of wire diameter. In the later instances, the mesh is made stronger (more steel per unit area) and the speed of the block must increase to perforate the mesh.

7 Example of Prediction of the Bullet Effect

The significance of the proposed scaling relationship resides in its predictive capacity. If test data corresponding to one point in Fig. 7 are known, then without additional testing, the performance of a wide range of other barriers can be immediately estimated using curves similar to those presented in the figure, regardless of the particular values for the block size, mesh characteristics, and system stiffness. In this section, such an approach is tested using numerical data presented by Cazzani et al. (2002) for a full barrier with height $H = 3$ m (see Fig. 12a), square mesh cell (as opposed to diamond shape before), and spherical blocks. The variables assumed in the previous study are given in Table 5.

A calibration process is employed to determine stiffness K for the system analyzed by Cazzani et al. (2002), who considered the full barrier rather than the simplified equivalent described in this paper. First, it is recognized that variables assumed previously with a block size of $D_b = 1.3$ m yield a value of $G^* = 0.0098$, which is very close to the value for one of the trend lines from Fig. 7 ($D_b = 0.55$ m; $G^* = 0.0092$). Considering the two values of G^* to be sufficiently close, the objective is then to find the value of K which causes the parameters E^* and S^*, as evaluated from the data of Cazzani et al., to fall on the trend line from Fig. 7, given by

$$E^* = 920(S^*)^{-1.65} \tag{10}$$

In this way, the equivalent stiffness for the full barrier of Cazzani et al. can be iteratively computed as $K = 8.1$ kN/m, which corresponds to $S^* = 1.8$.

Upon determining K, the critical velocities for smaller blocks (diameters of 1, 0.75, 0.5, and 0.3 m) can be predicted using the trends from Fig. 7 ($0.008 \leq G^* \leq 0.0164$), the equations of which are presented in Table 6. Note that the two smallest blocks used by Cazzani et al.

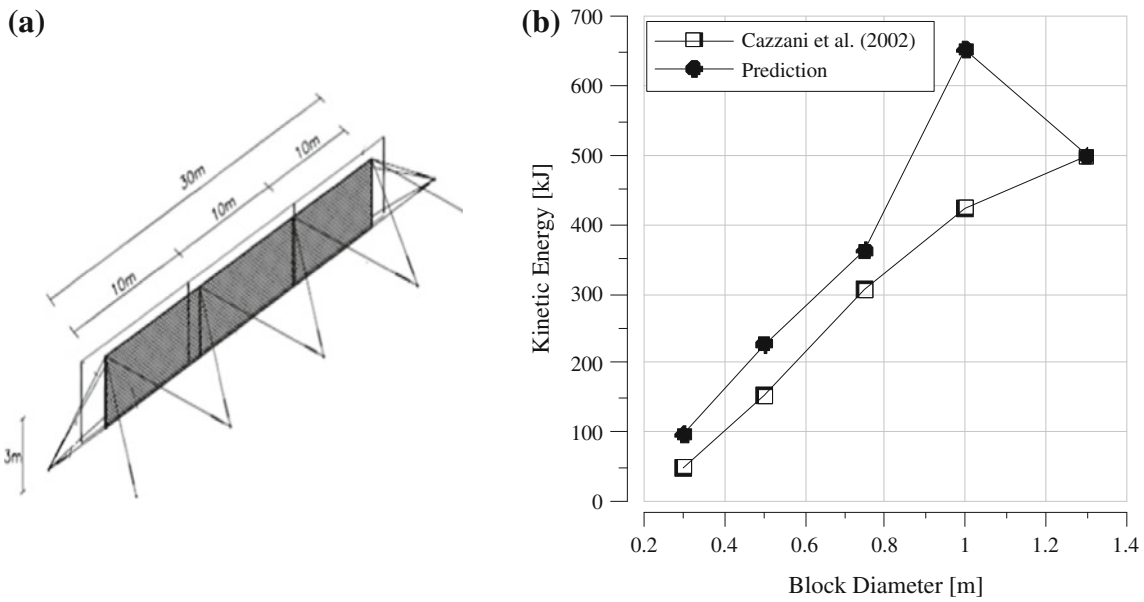

Fig. 12 **a** View of the full barrier used by Cazzani et al. (2002). **b** Evolution of kinetic energy at failure as function of block diameter: original numerical data by Cazzani et al. (2002) and prediction using the RoBaP model

Table 5 Variables assumed by Cazzani et al. (2002) and used in the prediction exercise

H (m)	ρ (kg/m^3)	A (m)	D_w (mm)	σ_y (MPa)	Block diameter D_b (m)
3	2,600	0.2	8	1,500	0.3, 0.5, 0.75, 1.0, 1.3

Table 6 Block diameters used by Cazzani et al. (2002) with corresponding values of G^* and roughly applicable trend lines from the present study

D_b (m) from Cazzani et al.	G^* from Cazzani et al.	G^* from the present study	Equation of trend line
1	0.0120	0.0116	$E^* = 2,663(S^*)^{-1.67}$
0.75	0.0148	0.0128	$E^* = 3,387(S^*)^{-1.64}$
0.5	0.0201	0.02	$E^* = 6,747(S^*)^{-1.50}$
0.3	0.0295	0.0295	$E^* = 11,871(S^*)^{-1.32}$

($D_b = 0.3$ and 0.5 m) correspond to $G^* = 0.2$ and 0.295, respectively, which are out of the initial range obtained in Fig. 7. To investigate these cases, two other trends were defined by running more simulations as previously.

The equations presented in Table 6 can be used to determine E^* for each block, and from this value of E^*, the critical speed and the kinetic energy can also be predicted. As the bullet effect is best seen when expressing the performance of the barrier in terms of kinetic energy, Fig. 12b compares the values of kinetic energy obtained by Cazzani et al. (2002) to those predicted by the proposed scaling relationship.

The predictive capacity of the scaling relationship when applied to the bullet effect can be clearly seen in Fig. 12b. The calibration was performed based on the block with $D_b = 1.3$ m, and hence there is a perfect match. Except for the block with $D_b = 1.0$ m, which is clearly abnormal, the values of kinetic energy are predicted relatively well. In particular, the progressive loss of performance (a reflection of the bullet effect) is well captured. One might argue that the increase of kinetic energy from $D_b = 1.3$–1 m displays a flaw in the proposed scaling relationship. However, one must bear in mind that the scaling relationship does not rely on the concept of kinetic energy, and there is no condition that kinetic energy cannot increase as the block size is reduced. Also, the critical speed for the anomalous point has been somewhat overestimated due to some approximations made during this prediction exercise, and this projects into the estimation of kinetic energy.

8 Conclusions

The scaling relationship proposed in this paper, alternatively referred to as the RoBaP Model, provides a novel means for quantifying the capacity of rockfall barriers to withstand impact from rock blocks. The model is expressed in terms of three key dimensionless parameters that combine the most important physical variables involved in barrier impact, including those for block size, barrier stiffness, mesh geometry, and yield strength of the mesh.

As the basis for the RoBaP Model, it is shown that these three dimensionless parameters are strongly correlated, with the correlations established based on results from a large number of numerical simulations performed using the finite element code ABAQUS/Explicit. In addition to providing a concise means for representing barrier performance over a range of variables, the RoBaP Model encapsulates the so-called bullet effect referring to the reduction in kinetic energy required to perforate a mesh as the block size decreases. The ability of the model to capture the bullet effect is demonstrated through an explicit example from literature where performance of a full rockfall protection barrier was investigated. In this example, the predicted values of kinetic energy are fairly close to the data presented in the previous study and, most importantly, the decrease in kinetic energy at failure with decreasing block size is well captured.

Prior to this study, there was no efficient and practical tool for the practitioners to estimate the performance of barriers when impacted by blocks of different size. With the RoBaP Model, test results for a single block size provide sufficient information to predict the performance for other block sizes. Since experiments and numerical simulations are typically performed at great expense in terms of cost and/or time, this predictive capability of the model is invaluable.

The RoBaP Model can be represented graphically as a network of curves relating the so-called performance parameter (E^*), the strength-stiffness parameter (S^*), and the geometrical parameter (G^*). The performance parameter E^* quantifies the impact resistance of a barrier, and it is not directly related to kinetic energy, but rather to the critical block speed required to fail the barrier. The parameter S^* characterizes the extent to which a barrier deforms prior to failure, and G^* describes the local geometry of the mesh in relation to the block size. As shown in Fig. 11, E^* and S^* are linearly related on a log–log scale, and an increase in G^* causes an upward shift of the E^*–S^* lines on such a plot. Mathematically, the relationship between E^*, S^*, and G^* is defined by the function F (see Eq. 6); however, an appropriate form for the full function F is yet to be determined. Determining F is left for future study, where additional data including that from experiments might be utilized to verify the current numerical trends. Indeed, slight differences can be expected because of the inherent simplifications of the numerical modeling (e.g., elastic-perfectly plastic behavior, connections between elements of the system).

The existence of the bullet effect suggests that no single value of kinetic energy (design value) can satisfactorily quantify barrier performance over a range of block sizes. The dependence of the design value on block size can be attributed to the presence of both elastic and plastic mechanisms of energy dissipation. For large blocks, the kinetic energy is primarily dissipated within deformation occurring in the barrier as a whole, and for small blocks, localized plastic failures occur. The results of this study suggest that kinetic energy as used in barrier performance criteria should perhaps be abandoned in favor of the critical speed, so that the analyst is automatically forced to think in terms of "performance curves" rather than unique design values. This paper is a first attempt to generate such dimensionless performance curves.

References

Anderheggen E, Volkwein A, Grassl H (2002) Numerical simulation of highly flexible rockfall protection systems. In: Proceedings of Fifth World Congress on Computational Mechanics. Vienna, Austria

Arndt B, Ortiz T, Turner AK (2009) Colorado's full-scale field testing of rockfall attenuator systems. Transp Res E-Circular, E-C141. Transportation Research Board, Colorado

Bertolo P, Oggeri C, Peila D (2009) Full-scale testing of draped nets for rock fall protection. Can Geotech J 46(3):306–317. doi:10.1139/T08-126

Buckingham E (1914) On physically similar systems: illustrations of the use of dimensional analysis. Phys Rev 4:345–376

Buzzi O, Giacomini A, Spadari M, Fityus S (2011) Numerical modeling of a rock fall mesh perforation upon impact. In: Proceedings of the 13th International Conference of the IACMAG 2011. Sydney, Australia, pp 1141–1146

Cantarelli G, Giani GP, Gottardi G, Govoni L (2008) Modelling rockfall protection fences. In: The first world landslide forum—Proceedings. ICL, Tokyo, pp 103–108

Cazzani A, Mongiovì L, Frenez T (2002) Dynamic finite element analysis of interceptive devices for falling rocks. Int J Rock Mech Min Sci 39(3):303–321. doi:10.1016/s1365-1609(02)00037-0

De Col R, Cocco (1996) Motivazioni tecniche ed economiche per la standardizzazione di prove sulle opere paramassi nella Provincia Autonoma di Trento. In: Giornata di studio su "La protezione contro la caduta di massi dai versanti rocciosi". GEAM, Torino, pp 65–72

Descoeudres F, Montani Stoffel S, Böll A, Gerber W, Labiouse V (1999) Rockfalls. In: Coping study on disaster resilient infrastructure. IDNDR, Zurich, pp 37–47

Duffy JD, Smith DD (1990) Field tests and evaluation of rockfall restraining nets. No. CA/TL-90/05, Final Report. California Dept. of Transportation, San Luis Obispo

EOTA (2008) Guideline for European technical approval of falling rock protection kits (ETAG 027). Brussels

Gerber W (2001) Guideline for the approval of rockfall protection kits. Swiss Agency for the Environment, Forests and Landscape (SAEFL), Swiss Federal Research Institute, Berne

Giani GP (1992) Rock slope stability analysis. Balkema, Rotterdam

Grassl H, Volkwein A, Anderheggen E, Ammann WJ (2002) Steel-net rockfall protection—experimental and numerical simulation. In: Seventh International Conference on Structures Under Shock and Impact. Montreal, Canada, pp 143–153

Hearn G, Barrett RK, Henson HH (1995) Testing and modeling of two rockfall barriers. In: Transportation research record, vol. 1504. National Research Council, Washington, pp 1–11

Johnson W (1972) Impact strength of materials. Edward Arnold, London

Langhaar HL (1951) Dimensional analysis and theory of models. Wiley, New York

Li QM, Jones N (2000) On dimensionless numbers for dynamic plastic response of structural members. Arch Appl Mech 70(4):245–254

Peila D, Oggeri C (2005) Barriere paramassi a rete - Tecnologia e criteri pregettuali. GEAM, Torino

Peila D, Pelizza S, Sassudelli F (1998) Evaluation of behaviour of rockfall restraining nets by full scale tests. Rock Mech Rock Eng 31(1):1–24

Volkwein A (2005) Numerical Simulation of flexible rockfall protection systems. In: Proceedings of Computing in Civil Engineering. ASCE, Cancun

Volkwein A, Melis L, Haller B, Pfeifer R (2005) Protection from landslides and high speed rockfall events—reconstruction of Chapman's Peak Drive. In: IABSE Symposium Lisbon 2005. Structures and extrem events. IABSE Reports vol. 90, incl. CD: 8 p